

# A Machine Learning Approach for Rate Constants III: Application to the $\text{Cl}(^2\text{P}) + \text{CH}_4 \rightarrow \text{CH}_3 + \text{HCl}$ Reaction

Paul L. Houston,<sup>\*,†</sup> Apurba Nandi,<sup>‡</sup> and Joel M. Bowman<sup>\*,‡</sup>

<sup>†</sup>*Department of Chemistry and Chemical Biology, Cornell University, Ithaca, New York 14853, U.S.A. and Department of Chemistry and Biochemistry, Georgia Institute of Technology, Atlanta, Georgia 30332, U.S.A*

<sup>‡</sup>*Cherry L. Emerson Center for Scientific Computation and Department of Chemistry, Emory University, Atlanta, Georgia 30322, USA*

E-mail: plh2@cornell.edu; jmbowma@emory.edu

## Abstract

The temperature dependence of the thermal rate constant for the reaction  $\text{Cl}(^3\text{P}) + \text{CH}_4 \rightarrow \text{HCl} + \text{CH}_3$  is calculated using a Gaussian Process machine learning (ML) approach to train on and predict thermal rate constants over a large temperature range. Following procedures developed in two previous reports, we use a training dataset of approximately 40 reaction/potential surface combinations, each of which is used to calculate the corresponding data base of rate constant at approximately eight temperatures. For the current application, we train on the entire dataset and then predict the temperature dependence of the title reaction employing a “split” dataset for correction at low and high temperatures to capture both tunneling and recrossing. The results are an improvement on recent RPMD calculations compared to accurate quantum ones, using the same high-level ab initio potential energy surface. Both tunneling at low temperatures and recrossing at high temperatures are observed to influence the rate constants. Recrossing effects, which are not described by TST and even sophisticated tunneling corrections, do appear in experiment at temperatures above around 600 K. The ML results describe these effects and in fact merge at 600 K with RPMD results (which can describe recrossing), and both are close to experiment at the highest experimental temperatures.

# Introduction

Svante Arrhenius nearly turned away from chemistry twice during his early studies because of poor performance, but he went on to earn a Nobel Prize in the field for his work on electrolytic solutions. Of more relevance to the current topic is his paper in 1889 on the temperature dependence of reaction rates,<sup>1</sup> where he found that  $k(T) = Ae^{-E_a/kT}$  where  $A$  is a constant,  $T$  is the Kelvin temperature, and  $E_a$  is an activation energy. A major subsequent advance came from the development in 1935 by Henry Eyring, and by Merideth Evans and Michael Polyani of transition state theory (TST),<sup>2-4</sup> which associated the activation energy with the location of a dividing surface that separated the reactants from the products in the space of energy vs. configuration. For reactions that have a saddle point between reactants and products, the dividing surface typically includes the saddle point. The constant  $A$  is associated in TST with a ratio of partition functions.

The near-linear relationship between the log of the rate constant with  $(1/T)$  predicted by both the Arrhenius equation and TST is actually not observed for many reactions, particularly at low temperatures. This is because quantum mechanical tunneling is found to be important at low temperatures and results in an increase in the rate constant from the linear prediction. Early proposals for including tunneling effects in the theory of chemical reactions were based on one-dimensional potentials. Of particular relevance to what follows in this paper is Eckart’s early work,<sup>5</sup> which continues to be used,<sup>6-8</sup> because it gives an analytical and often accurate result.

However, to get agreement with exact quantum methods or with experiment, we need more sophisticated quantum mechanical (QM) approaches, even though they are more computationally demanding. These methods have mostly been applied to collinear reactions, as summarized in a useful compilation by Allison and Truhlar.<sup>9</sup> Three-dimensional calculations, notably for the  $H + H_2$  reaction,<sup>10</sup> have also been studied, and these demonstrate shortcomings of the one-dimensional Eckart model that include, for example, recrossing of the TST dividing surface, corner cutting tunneling paths, and vibrationally adiabatic ef-

fects. To incorporate these effects, a variety of QM approaches have been employed, including instanton methods,<sup>11,12</sup> VPT2-based semiclassical transition state theory,<sup>8,13–17</sup> reduced-dimensionality quantum methods,<sup>18–22</sup> a large-curvature, corner-cutting reaction path,<sup>9,23</sup> ring polymer molecular dynamics (RPMD),<sup>24,25</sup> and ring polymer instanton methods.<sup>26</sup> Exact direct methods have also been developed to obtain the rate constant,<sup>27</sup> for example using multi-configuration time-dependent Hartree (MCTDH) theory, at least for zero total angular momentum,<sup>28,29</sup> and then augmented by  $J$ -shifting.<sup>20</sup>

Until recently, none of these methods had been applied to the important  $\text{Cl}(^3P_{3/2}) + \text{CH}_4 \rightarrow \text{HCl} + \text{CH}_3$  reaction, a reaction important in assessing the effect of chlorofluorocarbons in stratospheric chemistry. Many experimental measurements are available, mostly in very good agreement with one another. Collectively these measurements span a large temperature range from roughly 180 to more than 1000 K. We will refer to these by the names of the first authors of the reports: Clyne,<sup>30</sup> Manning,<sup>31</sup> Michael,<sup>32</sup> Whytock,<sup>33</sup> Keyser,<sup>34</sup> Zahniser,<sup>35</sup> Ravishankara,<sup>36</sup> Heneghan,<sup>37</sup> Seeley,<sup>38</sup> Pilgrim,<sup>39</sup> and Bryukov.<sup>40</sup> High-level, CCSD(T)-based potential energy surfaces for this reaction have been reported by Czako and Bowman (CB),<sup>41</sup> and, quite recently, by Li and Liu (LL).<sup>42</sup> Substantial theoretical investigations have also been reported. Barker, Nguyen, and Stanton<sup>43</sup> have reported kinetic isotope effects in the reaction using *ab initio* semiclassical transition state theory, while Georgievskii and Klippenstein (GK)<sup>44</sup> have recently studied how tunneling is affected by the non-separability of the reaction coordinate from other modes. The approach of the latter report provides a method that substantially improves on the one-dimensional estimation of tunneling; the comparison with experiment in that paper was limited to temperatures below 300 K, where agreement is very good. We return to this recent work in the Discussion section below. Li and Liu<sup>42</sup> used their potential to perform RPMD calculations for estimation of the temperature dependent rate constant, though over a limited range and with only modest agreement with experiment. Subsequently, a “first principles” theory for the reaction was recently reported by Hoppe and Manthe (HM),<sup>45</sup> who used the LL potential in a fully QM

method to calculate the rate constant as a function of temperature up to 540 K. Going to higher temperatures was evidently not computationally feasible. Their results are essentially in exact agreement with the experimental data up to that temperature. Thus, from the perspective of theory, this reaction has acquired an especially important role for both the potential energy surface and the reaction dynamics/rate constant theory.

One aspect of this reaction that was not directly addressed by these theoretical approaches is the extent of recrossing at high temperature. Recall that recrossing refers to the reduction of the reaction flux predictions of TST, which, by assumption, ignores recrossing. Recrossing is due to multidimensional dynamical effects where flux that crosses the transition state dividing surface recrosses but back in the direction of reactants. We return to this effect here where we apply our Machine Learning (ML) approach to obtain bimolecular thermal rate constants over a large temperature range.<sup>46,47</sup> The motivation for this approach was given in detail in those papers and so is just briefly reviewed below. Other ML methods have subsequently been reported for reaction rates by Valleau and co-workers,<sup>48,49</sup> activation energies in an article by Lewis-Atwell, Townsend and Grayson,<sup>50</sup> and for activation energies and reaction mechanisms in publications by Green and colleagues.<sup>51,52</sup>

In our first paper<sup>46</sup> we proposed using ML to find a correction to the Eckart tunneling correction to TST. The great appeal of the Eckart correction is two-fold. First, it is often quite accurate and second it requires no more information than is needed for a standard TST calculation. Of course this is not an exact correction and more accurate methods (though short of “exact”) are available, as mentioned above. However, these methods require substantially more information about the potential energy surface (PES), ranging from an expansion of the PES around the saddle-point beyond the harmonic expansion needed in TST to a global PES needed in RPMD and the MCTDH quantum calculations. Our goal was to explore whether ML can be applied to correct the Eckart correction and achieve a substantial improvement in accuracy at virtually no additional cost and with no additional information needed about the PES. The ML approach we took followed the standard protocol of training

the desired quantity on a known database. For us the quantity is the correction to the Eckart tunneling correction and the database is a large set of (ideally) exact quantum rate constant calculations for a variety of chemical reactions. We discuss below the database we used. For the ML model we used Gaussian process (GP) regression, which we briefly review in the next section. We used the database of rate constants for 13 reaction/potential surface combinations at typically 8 different temperatures. We created this database by data mining the large compilation of tables of rate constants reported by Allison and Truhlar in 1998. The tables contained TST and exact quantum results for numerous collinear reactions, of which we selected a total of 52. Also, all parameters needed for an Eckart tunneling correction were given. From the TST, Eckart correction and exact results the correction to Eckart were calculated. Then GP was trained on the 52 reactions and testing was then done on a set of 39 reaction/potential surface combinations. The GP method, when averaged over all test reactions, was within 80% of the accurate answer, considerably better than TST (330%) and Eckart corrected TST (ECK) (110%). The test reactions included 5 one-dimensional symmetric  $A + BA$  reaction/surface combinations; 16 one-dimensional asymmetric  $A + BC$  reaction/surface combinations; 15 three-dimensional reaction/surface combinations, both symmetric and asymmetric; and three polyatomic reactions:  $O(^3P) + CH_4$ ,  $H + CH_4$ , and  $HH + OH$ . A challenge for future predictions is that the dataset is relatively small. A strategy, then, is to examine other reactions that are studied by accurate methods, to determine to what extent GP is effective in predicting the new rate constant, and then to add the new reaction to the dataset. In our second paper<sup>47</sup> we focused on the  $O(^3P) + HCl$  reaction on the  $^3A'$  and  $^3A''$  potential energy surfaces. In that paper we took a different approach. We trained on the entire original dataset and then predicted the rate constant of this reaction. As described in detail in that paper we split the entire data set into two datasets, as briefly reviewed in the next section in given in more detail in Supplementary material (SM). Here we simply note that at low temperatures the corrections to the Eckart tunneling correction are larger than one. This is expected, as the Eckart correction generally underestimates

tunneling, especially in the deep tunneling region. At high temperatures where there is virtually no Eckart correction, i.e., the correction is about unity, the correction to Eckart is less than one. This accounts for recrossing and where in general TST overestimates the rate constant.

In the next section we briefly summarize the computational approach we use. We then present new predictions of the rate constant for the  $\text{Cl}(^2\text{P}) + \text{CH}_4$  reaction. This reaction is a challenge for our ML approach both because its parameters are at the edge of those of the training set and because it brings up possible issues, such as spin-orbit coupling and Van der Waals wells in both the entrance and exit channels. Detailed comparisons are made with the GP results of this work and the results from GK<sup>44</sup> as well as with the QM results from HM<sup>45</sup> and the RPMD results from LL.<sup>42</sup> We then incorporate “learning” this reaction into the correction datasets and verify that when used with ML we do get good agreement with the experiment, as expected.

## Computational Approach

The specific approach we proposed<sup>46</sup> is summarized next. Let  $k(T)$  be an exact rate constant calculated over a temperature range and using a given PES, and let  $k^{TST}(T)$  be the conventional TST rate constant using the same PES. The approach we took earlier is to represent the exact rate constant by the equation

$$k(T) = [\kappa_{ECK}(T)k^{TST}(T)]\chi(T), \tag{1}$$

where  $\kappa_{ECK}(T)$  is the Eckart transmission coefficient.<sup>6,7,53</sup> and  $\chi(T)$  is the correction to the Eckart correction to produce agreement with the accurate rate constant. We reasoned that this approach is better than using ML on the exact  $k^{TST}(T)$  directly because  $\kappa_{ECK}(T)$  is both easy to obtain and generally gives realistic tunneling corrections. Thus, the hope is that the GP correction to the Eckart transmission coefficient is small and easy to “learn”. To

proceed with machine learning of  $\chi(T)$  we need the usual three elements, namely a *database* of exact rate constants, a set of *descriptors*, and a general *machine learning method* to train on the database. We described these in detail previously,<sup>46</sup> so we just briefly summarize these key elements here.

Critical for the success of the ML approach are the parameters that characterize a reaction. A starting choice includes the three parameters that are needed to obtain the Eckart transmission coefficient,<sup>6</sup> which, in reduced units, are

$$\alpha_1 = V_1/\omega_{im}, \quad (2)$$

$$\alpha_2 = V_2/\omega_{im}, \quad (3)$$

$$u^*(T) = \omega_{im}/(0.69307 T). \quad (4)$$

$V_1$  ( $V_2$ ) is the saddle point barrier height in  $\text{cm}^{-1}$  relative to the reactants (products), omitting the zero-point energy in both cases, and where the energy of the reactants is zero. In the case of the  $\text{Cl}(^2\text{P}) + \text{CH}_4$  reaction, the zero of energy is lowered by the spin-orbit stabilization of the  $\text{Cl}(^2\text{P}_{3/2})$  atom, about 0.84 kcal/mol. Using transition state (TS) value of 6.97 kcal/mol from the CCSD(T)/CBS value in Table 3 of GK, this gives a value of  $V_1 = (6.97 - (-0.84))$  kcal/mol = 2733  $\text{cm}^{-1}$ . We, as well as GK and HM, assume no spin-orbit splitting other than the reactants. Thus, again from the CCSD(T)/CBS value in Table 3 of GK,  $V_2 = (6.97 - 5.04)$  kcal/mol = 675.3  $\text{cm}^{-1}$ . Note that in both the entrance and exit channels we have assumed that the presence of Van der Waals wells does not affect the  $V_1$  and  $V_2$  parameters used for the Eckart correction. In short, we ignore these wells. We defer comments about the possible effect of these wells to the Discussion section. The value  $\omega_{im}$  is the magnitude of saddle point imaginary frequency (in  $\text{cm}^{-1}$ ), which, from Table 2 of GK is 1194  $\text{cm}^{-1}$ . The value 0.69307 is an energy conversion factor, equal to  $k_B/(hc)$ , and  $T$  is the temperature in Kelvin. Improvements were obtained by including an additional parameter, the skew angle,  $\beta$ , which identifies important mass and corner cutting and recrossing effects. In the case of



the  $\text{Cl}(^2\text{P}) + \text{CH}_4$  reaction, this value is  $\beta = 17.3 = 0.302$  radians. More details, particularly the values of these parameters for the training dataset, can be found in our recent paper.<sup>46</sup>

As noted previously,<sup>47</sup> it is a challenge to obtain high precision in fitting the entire  $\chi$  dataset of approximately 400  $\chi$  values because they have a very large range, from 0.2 to 25. As in the  $\text{O}(^3\text{P}) + \text{HCl}$  paper,<sup>47</sup> we thus decided to split the data into two clusters in a manner that would permit more precise GP training on each. The dividing line between the two clusters is at  $\chi$  equal to 3.0. The cluster with  $\chi$  greater than 3.0 is denoted the Large- $\chi$  set and the other cluster is denoted Small- $\chi$  set. Figure S1. in the Supplementary Material (SM) shows these  $\chi$  groups as a function of  $u^*$ .

Having now a set of descriptors,  $\alpha_1$ ,  $\alpha_2$ ,  $\omega_{im}$ , and  $\beta$ , as well as a dataset from ref. 46, we now turn to the learning method. Gaussian Process (GP) regression is a machine learning method whose goal is to produce a smooth interpolation between known data.<sup>54</sup> The working equation is given by

$$\chi(\mathbf{x}) = \mathbf{K}_x^\top \mathbf{K}^{-1} \chi_0, \quad (5)$$

where  $\mathbf{x}$  represents the set of descriptors. The known values of  $\chi$  are collected in the column vector denoted  $\chi_0$ .  $K(\mathbf{x}_i, \mathbf{x}_j)$  is the kernel matrix with elements at the database values of  $\mathbf{x}$  and where  $\mathbf{K}_x = [k(\mathbf{x}, \mathbf{x}_1) \cdots k(\mathbf{x}, \mathbf{x}_N)]^\top$ . In this expression  $\mathbf{x}$  is the value of the descriptors where  $\chi$  is to be evaluated. A popular choice for the kernel matrix is<sup>54-56</sup>

$$K(\mathbf{x}_i, \mathbf{x}_j) = \sigma^2 \exp\left(-\frac{d_{ij}^2}{2}\right) + \delta_{ij} \sigma_{noise}, \quad (6)$$

where  $d_{ij}$  is the distance between the two vectors  $\mathbf{x}_i/l$  and  $\mathbf{x}_j/l$ , where the hyper-parameters are  $l$  and  $\sigma$ . The length-scale parameter,  $l$  can be single length or one that depends on the descriptor; we use the latter.  $\delta_{ij} \sigma_{noise}$  is the noise term that is added to the diagonal of the covariance matrix. In principle, this term is not necessary for fitting, because the data are not noisy. However, adding noise can avoid ill-conditioning of the matrix, and, more generally enters parametrically into the optimization of the hyper-parameters according to

maximization of log-marginal-likelihood .<sup>54,57</sup>

$$\log \mathcal{L} = -\frac{1}{2} (\mathbf{g}^\top \mathbf{K}^{-1} \mathbf{g} + \log |\mathbf{K}| + N \log 2\pi) \quad (7)$$

Once the optimal hyper-parameters are determined, the GP model can predict the value of  $\chi$  using Eq. 5. In a practical sense, the hyper-parameters govern the smoothness of the interpolation, also known as prediction.

We performed this GP regression on the Small and Large- $\chi$  datasets using the routines contained in the Python Scikitlearn library, which includes optimization of the hyperparameters.<sup>58</sup> The inputs are the descriptors and the output is the trained  $\chi$ . As a reminder, the database for exact  $\chi$  values is developed largely from a 1998 compilation of rate constants<sup>9</sup> as well as from results from several more recent quantum calculations of rates constants for polyatomic reactions, such as  $\text{OH} + \text{H}_2$ ,  $\text{H} + \text{CH}_4$ , and  $\text{O} + \text{CH}_4$ , as described in detail previously.<sup>46</sup>

The Small- $\chi$  data-set has a total 360 data points, and for the work we described below we took all the points to fit the data-set using GP regression. The RMS error of this fitting is 0.14461. The Large- $\chi$  data-set has total 37 data points, which for ML is very small. In order to avoid over-fitting of this limited set, we used a noise value (see Eq. 6) of 50, larger than that used for the previously studied  $\text{O}(^3P) + \text{HCl}$  reaction. Noise values of 20 and 30 gave nearly identical results, as shown in Figure S4. of the SM.

## The $\text{Cl}(^2\text{P}_{3/2}) + \text{CH}_4 \rightarrow \text{HCl} + \text{CH}_3$ Reaction

The  $\text{Cl}(^2\text{P}_{3/2}) + \text{CH}_4$  reaction is a challenge for our ML approach, given the range and sparsity of our relatively small dataset. Recall that the dataset is largely based on collinear  $\text{A} + \text{BC}$  reactions, with only a few three-dimensional reactions. In particular, for this reaction, using the most accurate electronic energies,  $\alpha_1 = 2.61$  and  $\alpha_2 = 0.645$  so that  $\alpha_1 - \alpha_2 = 1.97$ . Our complete dataset does have values of  $\alpha_1$  greater than and less than this value of  $\alpha_1$ ; however,

the smallest value of  $\alpha_2$  in our dataset is 0.70. And in that case there are only six total entries with this value of  $\alpha_2$ . Fortunately, for these entries  $\alpha_1 = 2.94$  and the skew angle is 20 deg, which is close to skew angle,  $\beta$ , of 17.3 deg. Our data set for skew angle ranges from 17 to 89 deg. The value of  $\beta$  for the  $\text{Cl}(^2\text{P}_{3/2}) + \text{CH}_4 \rightarrow \text{HCl} + \text{CH}_3$  reaction is  $17.3^\circ$ , near the lower limit of the dataset. So the values of the descriptors for this reaction are at the edges of the training dataset. Thus, it is interesting to see if a strategy such as that used successfully in the  $\text{O}(^3\text{P}) + \text{HCl}$  reaction will work for  $\text{Cl}(^2\text{P}_{3/2}) + \text{CH}_4$ .

Then too, there is the question of when to use the results of the GP calculation on the Large- $\chi$  set and when to use those of the Small- $\chi$  dataset. Only at the lowest temperatures are the  $u^*$  values only found in the former, so one must make a transition between using the two sets that does not result in a discontinuity in the slope of the  $\log_{10}(k(T))$  vs  $1000/T$  plot. Here, we use a transition between the two sets based on the probability that a given  $u^*$  will be associated with one set rather than the other, as described in Section S-I of the SM along with some details of the GP calculations using each dataset. We used a different strategy in paper 2 where a weighted average of predicted  $\chi$  values was used for several temperatures.<sup>47</sup>

Table 1 provides a summary of the GP-predicted results along with TST and Eckart corrected TST and experiment. The TST result is calculated either by direct count of the rotational levels and degeneracies or by using classical formulae, with practically identical results for the temperatures listed. Our TST calculations are in agreement with those of HM and GK, following discussions with HM, as described in Section S-IV of the SM. The “accurate” value of the rate constant is taken as the result of a third-order polynomial fit to the experimental  $\log_{10}(k(t))$  vs  $1000/T$  plot, shown in Fig. S1 in Section S-II. As mentioned, the Eckart correction  $\kappa$  predicts only a factor of ca. 2 correction from the TST rate constant at the lowest temperatures and is otherwise close to unity (i.e., no correction). The GP calculation gives a further factor of ca. 5.9 correction at the lowest temperature, but falls somewhat short of the GP target factor, 10.2, that would be needed to provide agreement with experiment, i.e., “accurate”.

**Table 1: Results for GP Calculation**

T (K)	u*	TST (this work)	Eckart Corrctn. $\kappa$	GP Corrctn. $\chi$	$k_{GP}$	GP Target	$k_{expt.}$
150	10.00	$6.89 \times 10^{-17}$	1.98	5.93	$8.08 \times 10^{-16}$	10.20	$1.39 \times 10^{-15}$
200	7.53	$1.44 \times 10^{-15}$	1.62	2.60	$6.07 \times 10^{-15}$	5.43	$1.27 \times 10^{-14}$
300	5.02	$3.48 \times 10^{-14}$	1.34	0.89	$4.13 \times 10^{-14}$	2.33	$1.09 \times 10^{-13}$
400	3.77	$2.01 \times 10^{-13}$	1.23	0.64	$1.57 \times 10^{-13}$	1.60	$3.94 \times 10^{-13}$
500	3.01	$6.49 \times 10^{-13}$	1.17	0.58	$4.38 \times 10^{-13}$	1.28	$9.67 \times 10^{-13}$
600	2.51	$1.55 \times 10^{-12}$	1.13	0.55	$9.70 \times 10^{-13}$	1.07	$1.88 \times 10^{-12}$
700	2.15	$3.06 \times 10^{-12}$	1.11	0.54	$1.83 \times 10^{-12}$	0.92	$3.12 \times 10^{-12}$
800	1.88	$5.34 \times 10^{-12}$	1.09	0.53	$3.09 \times 10^{-12}$	0.80	$4.67 \times 10^{-12}$
900	1.67	$8.53 \times 10^{-12}$	1.08	0.52	$4.80 \times 10^{-12}$	0.70	$6.48 \times 10^{-12}$
950	1.59	$1.05 \times 10^{-11}$	1.07	0.52	$5.83 \times 10^{-12}$	0.66	$7.46 \times 10^{-12}$
1000	1.51	$1.28 \times 10^{-11}$	1.07	0.51	$7.00 \times 10^{-12}$	0.62	$8.48 \times 10^{-12}$
1100	1.37	$1.81 \times 10^{-11}$	1.06	0.51	$9.73 \times 10^{-12}$	0.55	$1.06 \times 10^{-11}$
1200	1.26	$2.46 \times 10^{-11}$	1.05	0.50	$1.30 \times 10^{-11}$	0.50	$1.29 \times 10^{-11}$
1300	1.16	$3.24 \times 10^{-11}$	1.05	0.50	$1.69 \times 10^{-11}$	0.45	$1.52 \times 10^{-11}$
1400	1.08	$4.15 \times 10^{-11}$	1.04	0.49	$2.13 \times 10^{-11}$	0.41	$1.76 \times 10^{-11}$
1500	1.00	$5.19 \times 10^{-11}$	1.04	0.49	$2.63 \times 10^{-11}$	0.37	$2.00 \times 10^{-11}$
1600	0.94	$6.36 \times 10^{-11}$	1.04	0.48	$3.18 \times 10^{-11}$	0.34	$2.24 \times 10^{-11}$
1700	0.89	$7.67 \times 10^{-11}$	1.04	0.48	$3.80 \times 10^{-11}$	0.31	$2.47 \times 10^{-11}$
1800	0.84	$9.10 \times 10^{-11}$	1.03	0.48	$4.47 \times 10^{-11}$	0.29	$2.71 \times 10^{-11}$
1900	0.79	$1.07 \times 10^{-10}$	1.03	0.47	$5.19 \times 10^{-11}$	0.27	$2.94 \times 10^{-11}$

Figure 1 shows the progression of our calculations. The blue line gives the TST result, whereas the dashed green line gives the Eckart-corrected TST result. As can be seen, there is very little difference between these two; the Eckart correction is small. The black line with error bars shows the results of the further correction from the GP calculation, whereas the solid green line gives the result of the fit to the experiment. The GP correction substantially improved the low-temperature rate constants but does not quite provide quantitative agreement with the experiment. (Note that the GP correction uses  $\chi$  values from the Large and Small  $\chi$  datasets as described in detail in the SM. At the lowest three temperatures of Table 1 the contributions from the Large- $\chi$  datasets are 87, 53, and 11 percent, respectively. At 400 K or above the contributions are less than 3 percent; at 700 K or above they are less than 0.5 percent.) Nevertheless, there is a major improvement over TST and also the Eckart

correction at both low and high temperatures. At high temperatures both TST and Eckart corrected TST overestimates the accurate result by about a factors of 2 - 5.

The representative error bars shown in Fig. 1 are caused by two sources, the uncertainties for the ML predictions using different noise values and the uncertainties for using differing methods for combining the small- and large- $\chi$  data sets. The former is smaller than the latter. Fig. S4 shows predictions for different noise values used in the large- $\chi$  set; the curves are close except at the lowest temperatures. A larger error, shown by the representative error bars in Fig. 1 comes from the latter error source. The method we used (see Section S-I) was not the only method we tested, and the representative error bars include uncertainty from the different methods.

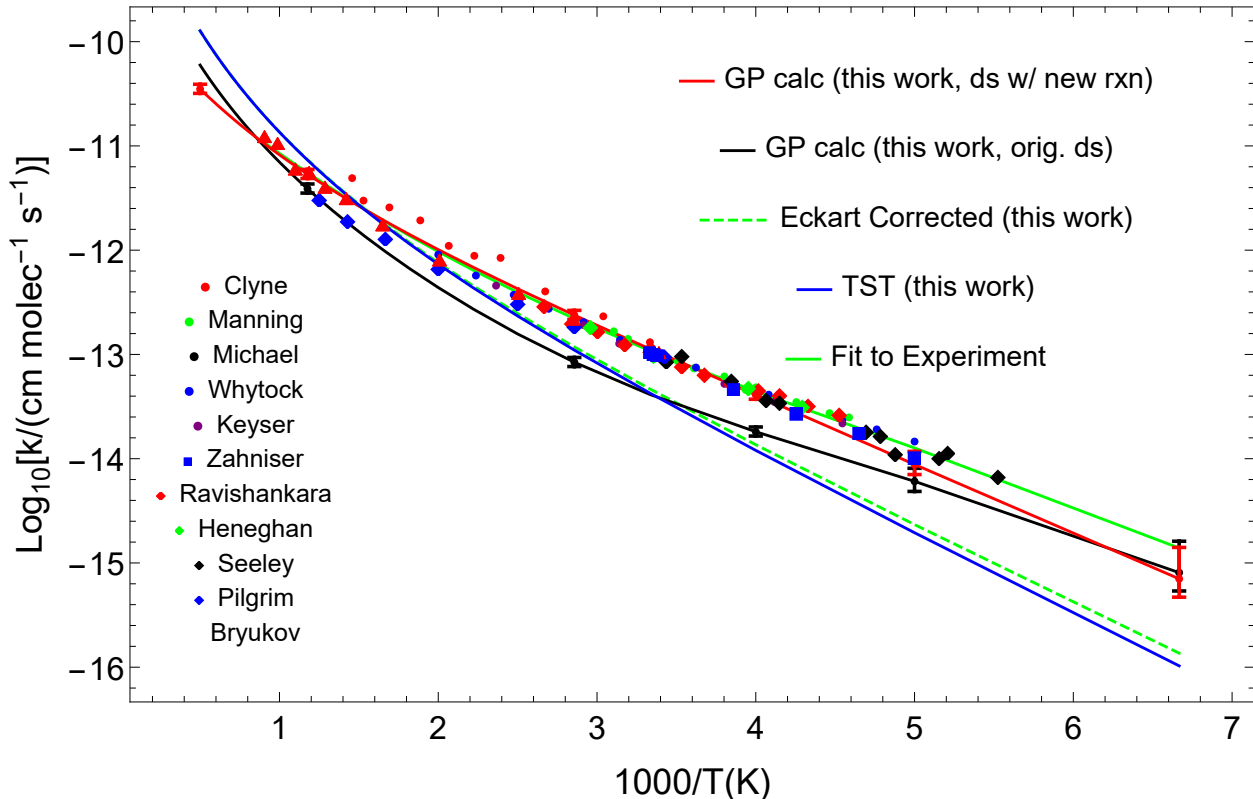


Figure 1:  $\text{Cl} + \text{CH}_4$  results for the GP method. The method starts with the TST rate constant (solid blue), performs a standard Eckart correction (producing the dashed green curve), and then performs a GP correction based on the original dataset (producing the solid black curve with representative error bars). If the  $\text{Cl} + \text{CH}_4$  reaction is included in the dataset, the GP calculation gives the solid red line, with representative error bars.

Of course, one goal of this study is to expand the dataset. The red line with error bars shows the GP result following augmentation of the training dataset with the data for the  $\text{Cl}(^2\text{P}_{3/2}) + \text{CH}_4$  reaction under investigation. When the reaction is included in the dataset with the target  $\chi$  values, the GP calculate reproduces the experimental data down to  $1000/T = 4$ , but then still underestimates slightly the needed correction at the lowest temperatures. We note that the data, the original GP calculation, and the GP calculation made with the augmented training dataset all predict lower rate constants at very high temperatures, when compared to the TST rate constants, correctly capturing the effect of recrossing trajectories.

## Discussion

Despite the small size of our training dataset, the partial coverage of it and other challenges posed by the  $\text{Cl}(^2\text{P}_{3/2}) + \text{CH}_4 \rightarrow \text{HCl} + \text{CH}_3$  reaction, the results shown above demonstrate that it is both possible to obtain an good prediction of the temperature dependence of a new reaction and that the prediction is improved substantially when the dataset is expanded by including the new reaction. We now investigate how the GP prediction compares with others.

Figure 2. shows a comparison of recent results from several groups. Liu and Li<sup>42</sup> used a machine-learning approach to develop a potential energy surface for the  $\text{Cl} + \text{CH}_4$  reaction and then performed RPMD calculations of the rate constant for several temperatures in a limited range. Their result is shown as the solid red line in the figure, which extends from  $1000/T = 0.5 - 5.0$ . The GP results from this work using the original training set are shown as the solid black line with representative error bars. The agreement between the two is good, but neither agrees perfectly with the experimental results, a sampling of which is shown along with the green line fit to all the experimental data. The results from the method of Georgievskii and Klippenstein<sup>44</sup> are shown in the dotted red line. Hoppe

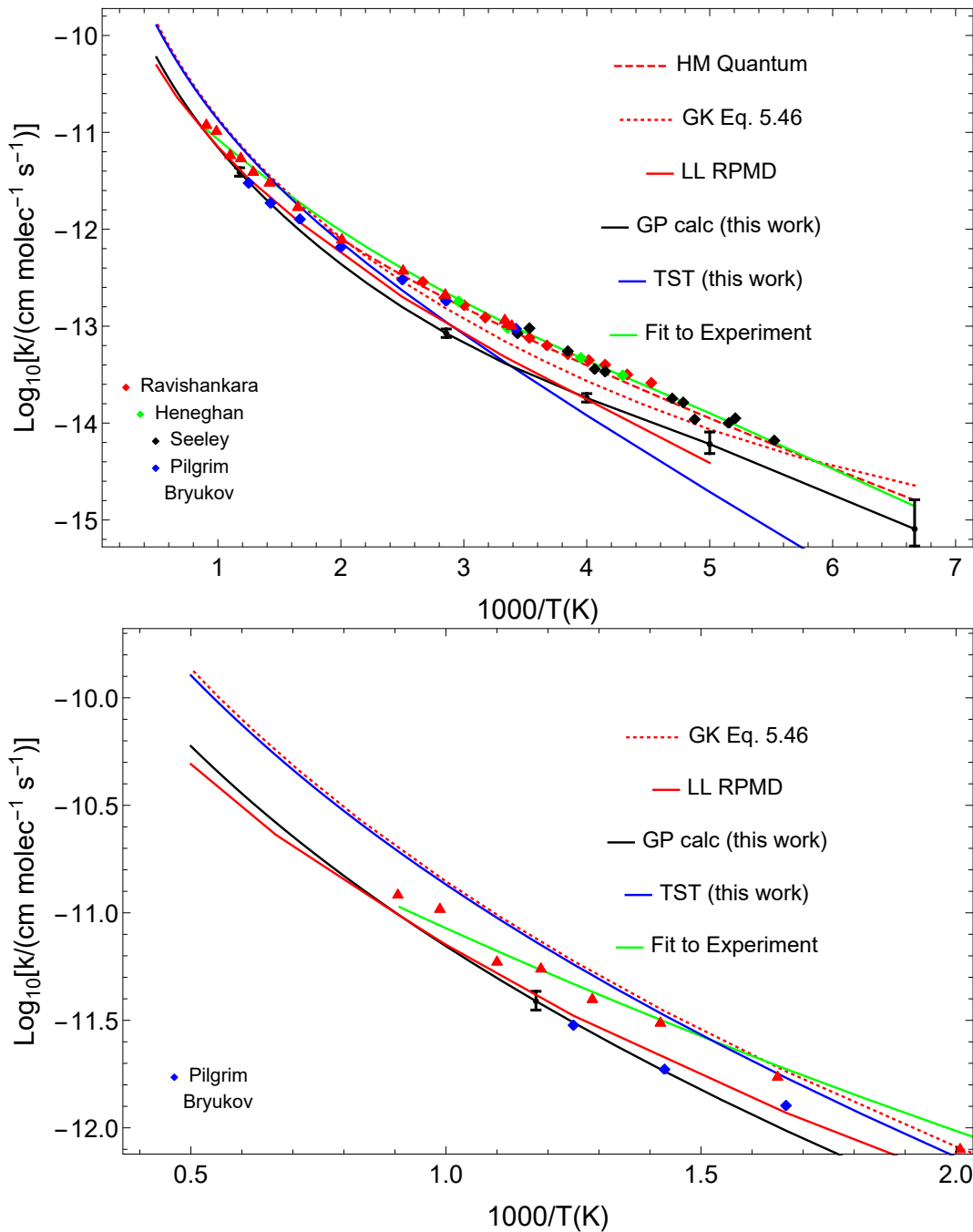


Figure 2: Top Panel: Comparison of results for the Cl + CH<sub>4</sub> reaction showing a sampling of experimental results and the fit to all the experimental data (solid green), the quantum results from ref. 37 (dashed red), the results from ref. 44 (dotted red), our GP results using the original training set (solid black), the RPMD results of ref. 42 (solid red), and the TST results (solid blue). Bottom Panel: Expansion of the High-T region.

and Manthe<sup>45</sup> used the LL PES to perform quantum calculations of the rate constant as a function of temperature, and their results are shown in the dashed red line extending from  $1000/T = 1.85 - 6.67$ . Both the GK and HH results are in relatively good agreement with the experiment, with the HM calculation being almost in exact agreement.

It is interesting to note that our GP results, using the original data set, and so a prediction, are in slightly in better overall agreement with experiment than the RPMD ones. The former requires only 4 parameters, a simple program, and a basic dataset; the calculation takes about a minute on a laptop. The latter calculation requires a full PES, a much more elaborate code, and a substantially longer calculation time. It is also curious that the RPMD calculation is not in better agreement with full QM calculation of HM, especially since both used the same PES. RPMD is essentially exact for the  $\text{H} + \text{CH}_4$  reaction<sup>59</sup> as shown in Figure. S4 of ref. 46, as well as for the  $\text{O} + \text{CH}_4$  reaction<sup>60</sup> as shown in Figure. 3 of ref. 46 and for the  $\text{O}(^3\text{P}) + \text{HCl}$  reaction<sup>61</sup> as shown in Figure. 9 of ref. 47. Whatever the answer is to this puzzle, it is clear that the GP method is effective in making a substantial correction to the TST or Eckart corrected TST rate constants, as we have seen in Figures. 1 and 2.

Another observation is that both our GP result and the data suggest that the rate constant is reduced at high temperatures compared to the TST result, likely because of recrossing. At first it seems surprising that neither the HM nor GK result captures this effect. In the HM study, the authors specifically commented that they did not see the trapped oscillatory motion of the H atom due to the heavy-light-heavy mass combination. However, it seems likely from Figure. 2 that their quantum calculation was not performed at high enough temperatures to observe this effect; the dashed red line giving their results stops at  $1000/T = 1.85$  or  $T = 540$  K,. The approach of GK, while effectively accounting for the tunneling, was not designed to cover recrossing. The RPMD calculation of LL and our GP calculation do appear to capture the effect, as shown most clearly in the bottom panel of Figure. 2. We do note that the GP predictions using the original datasets overestimates the extent of recrossing at temperatures between around 340 - 600 K.



Finally, we comment briefly on the possible effects of van der Waals wells in this reaction and in general. The importance of these for rate constants was perhaps noted first for the  $\text{O}(^3\text{P})+\text{HCl}$  reaction.<sup>61–63</sup> The reaction was the focus of a “stress test” for RPMD,<sup>61</sup> and as noted already it was one focus of our paper II in this series.<sup>47</sup> The fundamental effect is a quantum one, where resonances in these well enhance the reactivity at energies below the barrier and thus enhance tunneling. This quantum effect is not described in RPMD, and so the absence of this enhanced tunneling was suggested as the reason RPMD underestimates the exact quantum rate constant (on the same PES).<sup>61</sup> We don’t know if these effects are involved in the present reaction, which as noted does have van der Waals wells, and it is beyond the scope of this paper to investigate this issue. However, it is interesting to speculate on how these wells might be approximately incorporated into a 1d tunneling correction such as the Eckart correction. One of us presented a simple heuristic 1d model that treats the resonances as metastable states that increase tunneling through a 1d barrier.<sup>64</sup> That might be a first step towards such theory.

## Conclusions

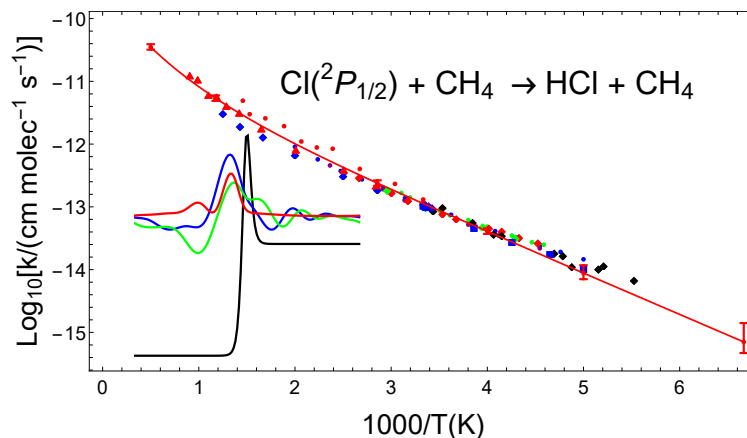
The Gaussian Process regression method for machine learning of thermal rate constants developed previously<sup>46,47</sup> has been shown here to provide a good estimate of the temperature dependence of the rate constant for the  $\text{Cl}(^2\text{P}_{3/2})+\text{CH}_4 \rightarrow \text{HCl} + \text{CH}_3$  reaction. The results suggest both that tunneling is important at temperatures below about 250 K and that recrossing is important at temperatures above about 500 K. The results are in fairly good agreement with RPMD calculations by Liu and Li,<sup>42</sup> but neither method is as accurate in predicting the experimental results as the predictions of the method used by Georgievskii and Klippenstein<sup>44</sup> or, especially, the quantum calculations of Hoppe and Manthe,<sup>45</sup> in the deep tunneling regime. However, the present ML and RMPD results are closer to experiment at higher temperatures, where recrossing becomes significant. When the new reaction is

included in the training dataset, the GP results are in agreement with experiment to within the error limits, suggesting that the new training set will be more effective in predicting rates for new three-dimensional systems in the future. We note that the original training basis set<sup>9</sup> was based predominantly on the results of one-dimensional reaction calculations. As more complex reactions are added to the dataset, we can expect improvements in the prediction of other reactions such as the  $\text{Cl} + \text{CH}_4$  one.

## Acknowledgments

JMB thanks NASA (grant 80NSSC20K0360) for financial support. We thank Yang Liu and Jun Li for providing their RPMD results, Hannes Hoppe and Uwe Manthe for providing their quantum and TST results and for extensive discussions, and Yuri Georgievskii and Stephen Klippenstein for providing the results of their Eq. 5.46.

## TOC Figure



## References

- (1) Arrhenius, S. Über die Reaktionsgeschwindigkeit bei der Inversion von Rohrzucker durch Säuren. *Z. Phys. Chem.* **1889**, *4U*, 226–248.
- (2) Eyring, H. The Activated Complex in Chemical Reactions. *J. Chem. Phys.* **1935**, *3*, 107–115.
- (3) Evans, M. G.; Polanyi, M. Some applications of the transition state method to the calculation of reaction velocities, especially in solution. *Trans. Faraday Soc.* **1935**, *31*, 875–894.
- (4) Laidler, K. J.; King, M. C. Development of transition-state theory. *J. Phys. Chem.* **1983**, *87*, 2657–2664.
- (5) Eckart, C. The Penetration of a Potential Barrier by Electrons. *Phys. Rev.* **1930**, *35*, 1303–1309.
- (6) Johnston, H. S.; Rapp, D. Large Tunnelling Corrections in Chemical Reaction Rates. II. *J. Am. Chem. Soc.* **1961**, *83*, 1–9.

- (7) Johnston, H. S.; Heicklen, J. Tunneling Corrections for Unsymmetrical Eckart Potential Energy Barriers. *J. Phys. Chem.* **1962**, *66*, 532–533.
- (8) Barker, J. R.; Nguyen, T. L.; Stanton, J. F. Kinetic Isotope Effects for  $\text{Cl} + \text{CH}_4 \rightarrow \text{HCl} + \text{CH}_3$  Calculated Using Ab Initio Semiclassical Transition State Theory. *J. Phys. Chem. A*. **2012**, *116*, 6408–19.
- (9) Allison, T. C.; Truhlar, D. G. In *Modern Methods for Multidimensional Dynamics Computations in Chemistry*; Thompson, D. L., Ed.; World Scientific: Singapore, 1998; pp 618–712.
- (10) Schatz, G. C.; Kuppermann, A. Quantum Mechanical Reactive Scattering for Three-Dimensional Atom Plus Diatom Systems. II. Accurate Cross Sections for  $\text{H} + \text{H}_2$ . *J. Chem. Phys.* **1976**, *65*, 4668–4692.
- (11) Miller, W. H. Semiclassical Limit of Quantum Mechanical Transition State Theory for Nonseparable Systems. *J. Chem. Phys.* **1975**, *62*, 1899–1906.
- (12) Zhao, Y.; Yamamoto, T.; Miller, W. H. Path Integral Calculation of Thermal Rate Constants within the Quantum Instanton Approximation: Application to the  $\text{H} + \text{CH}_4 \rightarrow \text{H}_2 + \text{CH}_3$  Hydrogen Abstraction Reaction in Full Cartesian Space. *J. Chem. Phys.* **2004**, *120*, 3100–3107.
- (13) Miller, W. H.; Hernandez, R.; Handy, N. C.; Jayatilaka, D.; Willetts, A. Ab initio Calculation of Anharmonic Constants for a Transition State, with Application to Semiclassical Transition State Tunneling Probabilities. *Chem. Phys. Lett.* **1990**, *172*, 62 – 68.
- (14) Hernandez, R.; Miller, W. H. Semiclassical Transition State Theory. A New Perspective. *Chem. Phys. Lett.* **1993**, *214*, 129 – 136.

- (15) Nguyen, T. L.; Stanton, J. F.; Barker, J. R. Ab Initio Reaction Rate Constants Computed Using Semiclassical Transition-State Theory:  $\text{HO} + \text{H}_2 \rightarrow \text{H}_2\text{O} + \text{H}$  and Isotopologues. *J. Phys. Chem. A*. **2011**, *115*, 5118–26.
- (16) Wagner, A. F. Improved Multidimensional Semiclassical Tunneling Theory. *J. Phys. Chem. A*. **2013**, *117*, 13089–100.
- (17) Clary, D. C. Spiers Memorial Lecture Introductory Lecture: Quantum Dynamics of Chemical Reactions. *Faraday Discuss.* **2018**, *212*, 9–32.
- (18) Bowman, J. M. *Adv. Chem. Phys.*; J. Wiley and Sons, Ltd, 1985; pp 115–167.
- (19) Bowman, J. M.; Wagner, A. F. In *The Theory of Chemical Reaction Dynamics*; Clary, D., Ed.; NATO ASI Series (Series C: Mathematical and Physical Sciences); Springer, Dordrecht, 1986; Vol. 170; Chapter 6, pp 129–164.
- (20) Bowman, J. M. Reduced Dimensionality Theory of Quantum Reactive Scattering. *J. Phys. Chem.* **1991**, *95*, 129–164.
- (21) Althorpe, S. C.; Clary, D. C. Quantum Scattering Calculations on Chemical Reactions. *Annu. Rev. Phys. Chem.* **2003**, *54*, 493–529.
- (22) von Horsten, H. F.; Banks, S. T.; Clary, D. C. An Efficient Route to Thermal Rate Constants in Reduced Dimensional Quantum Scattering Simulations: Applications to the Abstraction of Hydrogen from Alkanes. *J. Chem. Phys.* **2011**, *135*, 094311.
- (23) Marcus, R. A.; Coltrin, M. E. A New Tunneling Path for Reactions such as  $\text{H} + \text{H}_2 \rightarrow \text{H}_2 + \text{H}$ . *J. Chem. Phys.* **1977**, *67*, 2609–2613.
- (24) Craig, I. R.; Manolopoulos, D. E. Chemical Reaction Rates from Ring Polymer Molecular Dynamics. *J. Chem. Phys.* **2005**, *122*, 084106.

- (25) Suleimanov, Y. V.; de Tudela, R. P.; Jambrina, P. G.; Castillo, J. F.; Sajez-Rabanos, V.; Manolopoulos, D. E.; Aoiz, F. J. A Ring Polymer Molecular Dynamics Study of the Isotopologues of the  $\text{H}+\text{H}_2$  Reaction. *Phys. Chem. Chem. Phys.* **2013**, *15*, 3655–3665.
- (26) Richardson, J. O. Perspective: Ring-Polymer Instanton Theory. *J. Chem. Phys.* **2018**, *148*, 200901.
- (27) Miller, W. H.; Schwartz, S. D.; Tromp, J. W. Quantum Mechanical Rate Constants for Bimolecular Reactions. *J. Chem. Phys.* **1983**, *79*, 4889–4898.
- (28) Wu, T.; Werner, H.-J.; Manthe, U. First-Principles Theory for the  $\text{H} + \text{CH}_4 \rightarrow \text{H}_2 + \text{CH}_3$  Reaction. *Science* **2004**, *306*, 2227–2229.
- (29) Welsch, R.; Manthe, U. Reaction Dynamics with the Multi-Layer Multi-Configurational Time-Dependent Hartree Approach:  $\text{H} + \text{CH}_4 \rightarrow \text{H}_2 + \text{CH}_3$  Rate Constants for Different Potentials. *J. Chem. Phys.* **2012**, *137*, 244106.
- (30) Clyne, M. A. A.; Walker, R. F. Absolute Rate Constants for Elementary Reactions in the Chlorination of  $\text{CH}_4$ ,  $\text{CD}_4$ ,  $\text{CH}_3\text{Cl}$ ,  $\text{CH}_2\text{Cl}_2$ ,  $\text{CHCl}_3$ ,  $\text{CDCl}_3$  and  $\text{CBrCl}_3$ . *J. Chem. Soc., Faraday Trans. 1.* **1973**, *69*, 1547–1567.
- (31) Manning, R. G.; Kurylo, M. J. Flash Photolysis Resonance Fluorescence Investigation of the Temperature Dependencies of the Reactions of Chlorine(2P) Atoms with Methane, Chloromethane, Fluoromethane, Excited Fluoromethane, and Ethane. *J. Phys. Chem.* **1977**, *81*, 291–296.
- (32) Michael, J. V.; Lee, J. H. Selected Rate Constants for H, O, N, and Cl Atoms with Substrates at Room Temperatures. *Chem. Phys. Lett.* **1977**, *51*, 303–306.
- (33) Whytock, D. A.; Lee, J. H.; Michael, J. V.; Payne, W. A.; Stief, L. J. Absolute Rate of the Reaction of  $\text{Cl}(2\text{P})$  with Methane from 200–500 K. *J. Chem. Phys.* **1977**, *66*, 2690–2695.

- (34) Keyser, L. F. Absolute Rate and Temperature Dependence of the Reaction between Chlorine (2P) Atoms and Methane. *J. Chem. Phys.* **1978**, *69*, 214–218.
- (35) Zahniser, M. S.; Berquist, B. M.; Kaufman, F. Kinetics of the reaction  $\text{Cl} + \text{CH}_4 \rightarrow \text{CH}_3 + \text{HCl}$  from 200° to 500° K. *Int. J. Chem. Kinet.* **1978**, *10*, 15–29.
- (36) Ravishankara, A. R.; Wine, P. H. A Laser Flash Photolysis-Resonance Fluorescence Kinetics Study of the Reaction  $\text{Cl}(2\text{P}) + \text{CH}_4 \rightarrow \text{CH}_3 + \text{HCl}$ . *J. Chem. Phys.* **1980**, *72*, 25–30.
- (37) Heneghan, S. P.; Knoot, P. A.; Benson, S. W. The Temperature Coefficient of the Rates in the System  $\text{Cl} + \text{CH}_4 = \text{CH}_3 + \text{HCl}$ , Thermochemistry of the Methyl Radical. *Int. J. Chem. Kinet.* **1981**, *13*, 677–691.
- (38) Seeley, J. V.; Jayne, J. T.; Molina, M. J. Kinetic Studies of Chlorine Atom Reactions Using the Turbulent Flow Tube Technique. *J. Phys. Chem.* **1996**, *100*, 4019–4025.
- (39) Pilgrim, J. S.; McIlroy, A.; Taatjes, C. A. Kinetics of Cl Atom Reactions with Methane, Ethane, and Propane from 292 to 800 K. *J. Chem. Phys. A* **1997**, *101*, 1873–1880.
- (40) Bryukov, M. G.; Slagle, I. R.; Knyazev, V. D. Kinetics of Reactions of Cl Atoms with Methane and Chlorinated Methanes. *J. Chem. Phys. A* **2002**, *106*, 10532–10542.
- (41) Czako, G.; Bowman Joel, M. Dynamics of the Reaction of Methane with Chlorine Atom on an Accurate Potential Energy Surface. *Science* **2011**, *334*, 343–346.
- (42) Liu, Y.; Li, J. An Accurate Potential Energy Surface and Ring Polymer Molecular Dynamics Study of the  $\text{Cl} + \text{CH}_4 \rightarrow \text{HCl} + \text{CH}_3$  Reaction. *Phys. Chem. Chem. Phys.* **2020**, *22*, 344–353.
- (43) Barker, J. R.; Nguyen, T. L.; Stanton, J. F. Kinetic Isotope Effects for  $\text{Cl} + \text{CH}_4 = \text{HCl} + \text{CH}_3$  Calculated Using ab Initio Semiclassical Transition State Theory. *J. Chem. Phys. A* **2012**, *116*, 6408–6419.

- (44) Georgievskii, Y.; Klippenstein, S. J. Entanglement Effect and Angular Momentum Conservation in a Nonseparable Tunneling Treatment. *J. Chem. Theory Comput.* **2021**, *17*, 3863–3885.
- (45) Hoppe, H.; Manthe, U. First-Principles Theory for the Reaction of Chlorine with Methane. *J. Phys. Chem. Lett.* **2022**, *13*, 2563–2566.
- (46) Houston, P. L.; Nandi, A.; Bowman, J. M. A Machine Learning Approach for Prediction of Rate Constants. *J. Phys. Chem. Letts* **2019**, *10*, 5250–5258.
- (47) Nandi, A.; Bowman, J. M.; Houston, P. A Machine Learning Approach for Rate Constants. II. Clustering, Training, and Predictions for the  $\text{O}(3\text{P}) + \text{HCl} \rightarrow \text{OH} + \text{Cl}$  Reaction. *J. Phys. Chem. A* **2020**, *124*, 5746–5755.
- (48) Komp, E.; Valleau, S. Machine Learning Quantum Reaction Rate Constants. *J. Phys. Chem. A* **2020**, *124*, 8607–8613.
- (49) Komp, E.; Janulaitis, N.; Valleau, S. Progress towards Machine Learning Reaction Rate Constants. *Phys. Chem. Chem. Phys.* **2021**,
- (50) Lewis-Atwell, T.; Townsend, P. A.; Grayson, M. N. Machine Learning Activation Energies of Chemical Reactions. *WIREs. Comput. Mole. Sci.* **2021**, *n/a*, e1593.
- (51) Green, W. H. In *Computer Aided Chemical Engineering*; Faravelli, T., Manenti, F., Ranzi, E., Eds.; Elsevier, 2019; Vol. 45; pp 259–294.
- (52) Grambow, C. A.; Pattanaik, L.; Green, W. H. Deep Learning of Activation Energies. *J. Phys. Chem. Lett.* **2020**, *11*, 2992–2997.
- (53) Brown, R. L. A Method of Calculating Tunneling Corrections for Eckart Potential Barriers. *J. Res. Nat. Bur. Stand.* **1981**, *86*, 357–359.
- (54) Rasmussen, C. E.; Williams, C. K. I. *Gaussian processes for machine learning*; the MIT Press, 2006.



- (55) Vieira, D.; Krems, R. V. Rate Constants for Fine-structure Excitations in O–H Collisions with Error Bars Obtained by Machine Learning. *Astrophys. J.* **2017**, *835*, 255.
- (56) Bartók, A. P.; Csányi, G. Gaussian Approximation Potentials: A Brief Tutorial Introduction. *Int. J. Quantum Chem.* **2015**, *115*, 1051–1057.
- (57) Cui, J.; Krems, R. V. Efficient Non-Parametric Fitting of Potential Energy Surfaces for Polyatomic Molecules with Gaussian Processes. *J. Phys. B: At. Mol. Opt. Phys.* **2016**, *49*.
- (58) Pedregosa, F.; Varoquaux, G.; Gramfort, A.; Michel, V.; Thirion, B.; Grisel, O.; Blondel, M.; Prettenhofer, P.; Weiss, R.; Dubourg, V. et al. Scikit-learn: Machine Learning in Python. *J. Mach. Learn. Res.* **2011**, *12*, 2825–2830.
- (59) Meng, Q.; Chen, J.; Zhang, D. H. Communication: Rate Coefficients of the  $\text{H} + \text{CH}_4 \rightarrow \text{H}_2 + \text{CH}_3$  Reaction from Ring Polymer Molecular Dynamics on a Highly Accurate Potential Energy Surface. *J. Chem. Phys.* **2015**, *143*, 101102.
- (60) Li, Y.; Suleimanov, Y. V.; Green, W. H.; Guo, H. Quantum Rate Coefficients and Kinetic Isotope Effect for the Reaction  $\text{Cl} + \text{CH}_4 \rightarrow \text{HCl} + \text{CH}_3$  from Ring Polymer Molecular Dynamics. *J. Phys. Chem. A.* **2014**, *118*, 1989–1996.
- (61) Menendez, M.; Jambrina, P. G.; Zanchet, A.; Verdasco, E.; Suleimanov, Y. V.; Aoiz, F. J. New Stress Test for Ring Polymer Molecular Dynamics: Rate Coefficients of the  $\text{O}(^3\text{P}) + \text{HCl}$  Reaction and Comparison with Quantum Mechanical and Quasi-classical Trajectory Results. *J. Phys. Chem. A.* **2019**, *123*, 7920–7931.
- (62) Xie, T.; Wang, D.; Bowman, J. M.; Manolopoulos, D. E. Resonances in the  $\text{O}(^3\text{P}) + \text{HCl}$  Reaction Due to Van der Waals Minima. *J. Chem. Phys.* **2002**, *116*, 7461–7467.
- (63) Xie, T.; Bowman, J. M.; Peterson, K. A.; Ramachandran, B. Quantum Calculations of

the Rate Constant for the  $\text{O}(^3\text{P})+\text{HCl}$  Reaction on New Ab initio  $\text{A}'$  and  $\text{A}''$  Surfaces.  
*J. Chem. Phys.* **2003**, *119*, 9601–9608.

- (64) Bowman, J. M. Enhancement of Tunneling Due to Resonances in Pre-barrier Wells in Chemical Reactions. *Chem. Phys.* **2005**, *308*, 255 – 257.

# **Supplementary Material: A Machine Learning Approach for Rate Constants III: Application to the $\text{Cl}(^2\text{P})+\text{CH}_4\rightarrow\text{CH}_3+\text{HCl}$ Reaction**

Paul L. Houston,<sup>\*,†</sup> Apurba Nandi,<sup>‡</sup> and Joel M. Bowman<sup>\*,‡</sup>

<sup>†</sup>*Department of Chemistry and Chemical Biology, Cornell University, Ithaca, New York  
14853, U.S.A. and Department of Chemistry and Biochemistry, Georgia Institute of  
Technology, Atlanta, Georgia 30332, U.S.A*

<sup>‡</sup>*Cherry L. Emerson Center for Scientific Computation and Department of Chemistry,  
Emory University, Atlanta, Georgia 30322, USA*

E-mail: plh2@cornell.edu; jmbowma@emory.edu

## Contents

### S-I. Experimental Data

The available experimental data are shown in Figure S1. For use in other figures in the main text, the green line in the figure shows a fit to the data of a third-order polynomial. Experimental data are identified by the first author: Clyne,<sup>1</sup> Manning,<sup>2</sup> Michael,<sup>3</sup> Whytock,<sup>4</sup> Keyser,<sup>5</sup> Zahniser,<sup>6</sup> Ravishankara,<sup>7</sup> Heneghan,<sup>8</sup> Seeley,<sup>9</sup> Pilgrim,<sup>10</sup> and Bryukov.<sup>11</sup>

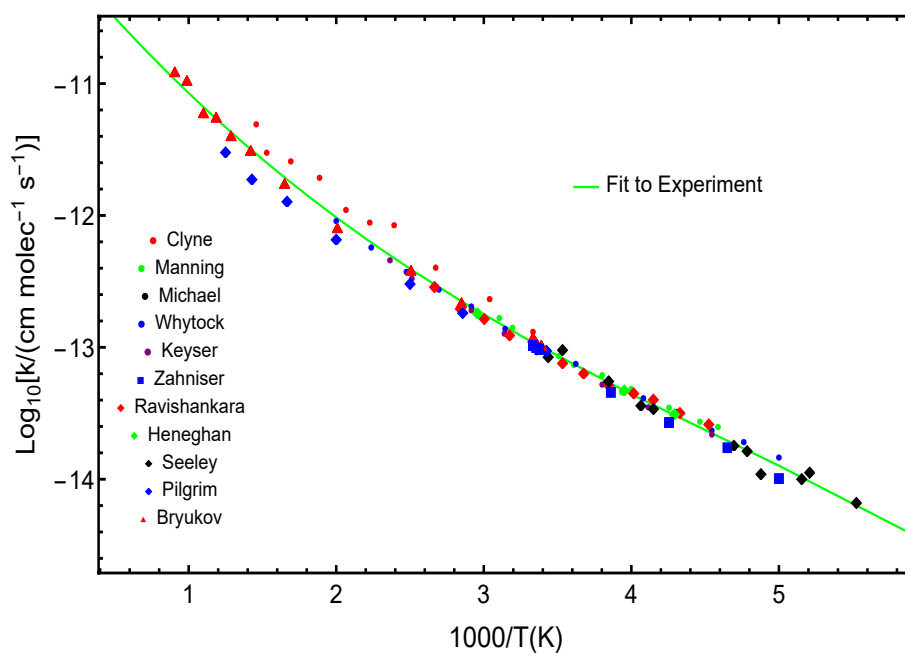


Figure S1: A fit of  $\text{Log}_{10}(k)$  vs  $1000/T$  for the experimental data to a  $3^{\text{rd}}$ -order polynomial. The fit is used to represent the experiment in some plots of the main text.

## S-II. Computational Details

Figure. S2 shows values of  $\chi$  as a function of  $u^*$  for the entire data set, which is largely based on a compilation by Allison and Truhlar.<sup>12</sup> Several features are important to note in this plot, where values of  $\chi$  larger than 3.0 are shown in blue, while values lower than 3.0 are shown in red. There is a region of overlap between the two clusters for  $u^*$  in the range of approximately 6 to 13. Values of  $u^*$  below 5 appear only in the small- $\chi$  cluster and values of  $u^*$  above 13 appear only in large- $\chi$  cluster. The question we now address is which cluster of  $\chi$  should we use at a given value of  $u^*$ . In previous work<sup>13</sup> we adopted the simple expedient of using the small- $\chi$  values for temperatures corresponding to  $u^*$  below 13, where the  $\chi$  values were either solely in the small- $\chi$  group or where the two groups overlapped, and the large- $\chi$  values for temperatures corresponding to  $u^*$  above 13, where the  $\chi$  values were solely from the large- $\chi$  group. Here we use a somewhat more nuanced approach.

It is clear from Fig. S2 that we should use almost exclusively the large- $\chi$  values above  $u^*=13$  and the almost exclusively the small- $\chi$  values below  $u^*=5$ . What we seek is a method for evaluating  $\chi$  more equitably, especially in the overlap region. We approach this by noting that we can assign a raw probability (or equivalently a weight) for using the low- $\chi$  value as being the fraction of low- $\chi$  values that are above of the desired  $u^*$ . Similarly, a raw probability for using the high- $\chi$  value can be assigned to the fraction of high- $\chi$  values that are below the desired  $u^*$ . Let these raw probabilities be  $P_{high}(u^*)$  and  $P_{low}(u^*)$ . Each is normalized within its own group, but the two probabilities are not yet normalized to one another. The correct normalization is such that  $P_{high}^{norm}(u^*) + P_{low}^{norm}(u^*) = 1$ , and we achieve this with the equations

$$P_{high}^{norm}(u^*) = \frac{P_{high}(u^*)}{P_{high}(u^*) + P_{low}(u^*)} \quad (S1)$$

$$P_{low}^{norm}(u^*) = \frac{P_{low}(u^*)}{P_{high}(u^*) + P_{low}(u^*)} \quad (S2)$$

S3

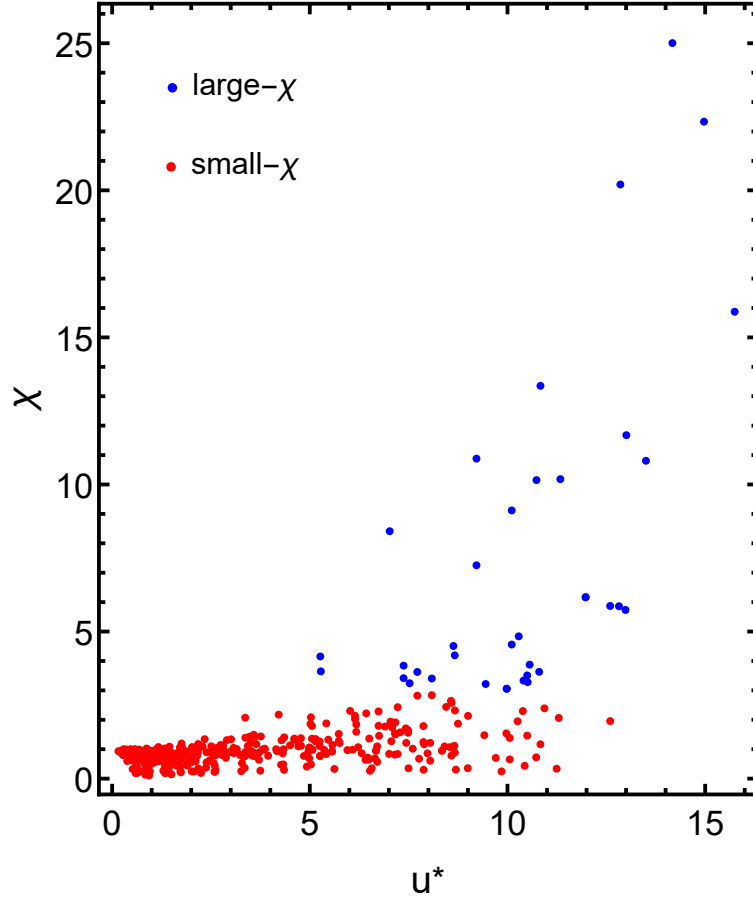


Figure S2:  $\chi$  as a function of  $u^*$  the entire dataset. Values above  $\chi = 3.0$  are shown in blue; those below 3.0 are shown in red.

In practice, we calculate  $P_{high}(u^*)$  and  $P_{low}(u^*)$  from the positions of the points in Figure S2, simply by automatic counting, and then fit the counts in each case by a suitable function that can then be used in Eqs. (S1) and (S2).

Figure S3 shows the values of  $P_{high}^{norm}(u^*)$  in blue and  $P_{low}^{norm}(u^*)$  in red. As expected,  $P_{high}^{norm}(u^*)$  approaches unity above  $u^*=13$ , whereas  $P_{low}^{norm}(u^*)$  approaches unity below  $u^*=5$ . The probabilities are equal at approximately  $u^*=7.5$ , or a temperature (for the Cl

+ CH<sub>4</sub> reaction) of approximately 200 K. Thus, only the very lowest temperatures have substantial contribution from  $P_{high}^{norm}(u^*)$ . To find the value of  $\chi$  for any value of  $u^*$ , we use the formula

$$\chi(u^*) = P_{high}^{norm}(u^*)\chi_{high}(u^*) + P_{low}^{norm}(u^*)\chi_{low}(u^*) \quad (S3)$$

where  $\chi_{high}(u^*)$  and  $\chi_{low}(u^*)$  are the values calculated using the Gaussian Process procedure.

Figure. S4 shows an exploration of the effect of the noise level in Equation (6) of the main text on the GP prediction of the rate constant. Values of  $\sigma_{noise} = 20, 30$ , and  $50$  were examined. The figure shows the predictions for these values as well as the TST rate constant (solid blue) and the fit to experiment (solid green). There is little difference between the results; we chose the  $50$  value because it was slightly better at low temperatures.

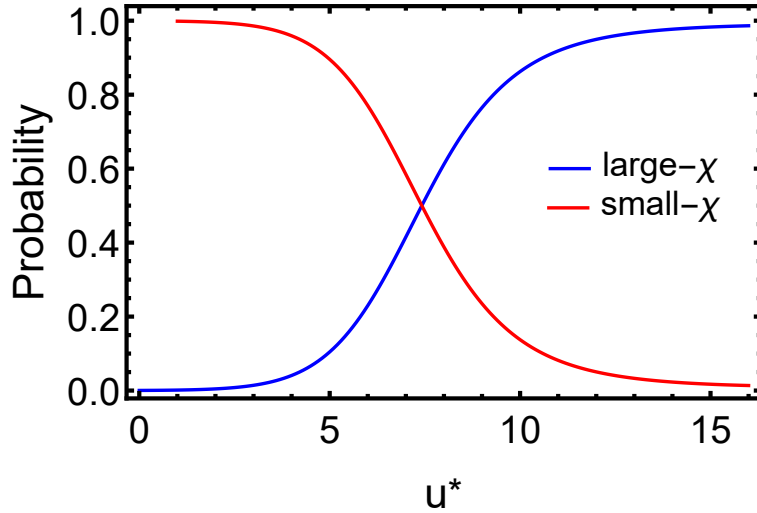


Figure S3: As a function of  $u^*$ , the plot shows the probability of using the GP value for the large- $\chi$  cluster (blue) or the small- $\chi$  cluster (red).

S5

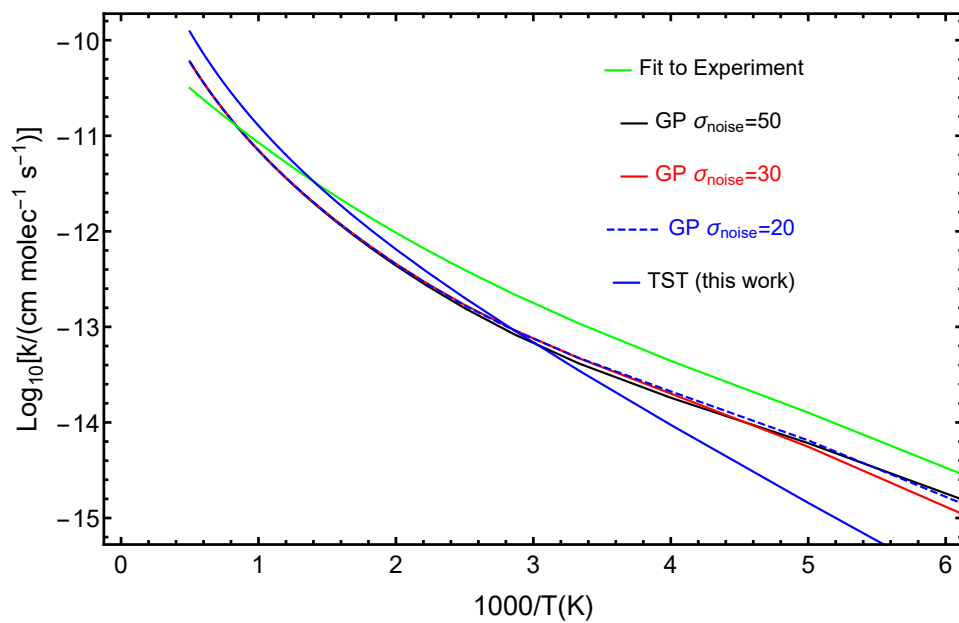


Figure S4: Gaussian Process predictions of the  $\text{Cl} + \text{CH}_4$  rate constant for three different values,  $\sigma_{\text{noise}}$ , of the noise parameter in Equation (6) of the main text. The figure also shows the TST rate constants and the fit to the experimental rate constants.



### S-III. TST Rate Constant

Both Hoppe and Manthe (HM)<sup>14</sup> and Georgievskii and Klippenstein (GK)<sup>15</sup> have previously published calculations of the Transition State Theory (TST) rate constant as a function of temperature. The parameters for the barrier height to the forward reaction, the imaginary frequency of the barrier, and the barrier height for the reverse reaction are all similar. In neither case did the result of the TST calculation affect their final results, which were both in good agreement with experiment. Because our calculation starts from the TST result, and then corrects that result first with a simple Eckart correction and then with the Gaussian Process (GP) result, it is important for our method that we start with an accurate TST result. Unfortunately, the HM and GK TST results as published are not in good agreement with one another. We thus performed our own TST calculations, both treating the rotational partition function classically and evaluating it by direct count. Important references, particularly concerning the direct count, symmetry factors, and nuclear spin statistics, are those by McDowell<sup>16,17</sup> and Herzberg.<sup>18</sup> After correcting errors in our own calculation concerning nuclear spin degeneracies, and after identifying a zero-point energy error on their part, conversations with Hoppe and Manthe led us to agreement between their method and our methods, and fortunately all of them agreed with the result of GK. The result from our own calculation that we show in the figures in the main text, is nearly identical to that of GK.

## References

- (1) Clyne, M. A. A.; Walker, R. F. Absolute Rate Constants for Elementary Reactions in the Chlorination of  $\text{CH}_4$ ,  $\text{CD}_4$ ,  $\text{CH}_3\text{Cl}$ ,  $\text{CH}_2\text{Cl}_2$ ,  $\text{CHCl}_3$ ,  $\text{CDCl}_3$  and  $\text{CBrCl}_3$ . *J. Chem. Soc., Faraday Trans. 1.* **1973**, *69*, 1547–1567.
- (2) Manning, R. G.; Kurylo, M. J. Flash Photolysis Resonance Fluorescence Investigation of the Temperature Dependencies of the Reactions of Chlorine(2P) Atoms with Methane, Chloromethane, Fluoromethane, Excited Fluoromethane, and Ethane. *J. Phys. Chem.* **1977**, *81*, 291–296.
- (3) Michael, J. V.; Lee, J. H. Selected Rate Constants for H, O, N, and Cl Atoms with Substrates at Room Temperatures. *Chem. Phys. Lett.* **1977**, *51*, 303–306.
- (4) Whytock, D. A.; Lee, J. H.; Michael, J. V.; Payne, W. A.; Stief, L. J. Absolute Rate of the Reaction of Cl(2P) with Methane from 200–500 K. *J. Chem. Phys.* **1977**, *66*, 2690–2695.
- (5) Keyser, L. F. Absolute Rate and Temperature Dependence of the Reaction between Chlorine (2P) Atoms and Methane. *J. Chem. Phys.* **1978**, *69*, 214–218.
- (6) Zahniser, M. S.; Berquist, B. M.; Kaufman, F. Kinetics of the reaction  $\text{Cl} + \text{CH}_4 \rightarrow \text{CH}_3 + \text{HCl}$  from 200° to 500° K. *Int. J. Chem. Kinet.* **1978**, *10*, 15–29.
- (7) Ravishankara, A. R.; Wine, P. H. A Laser Flash Photolysis-Resonance Fluorescence Kinetics Study of the Reaction  $\text{Cl}(2\text{P}) + \text{CH}_4 \rightarrow \text{CH}_3 + \text{HCl}$ . *J. Chem. Phys.* **1980**, *72*, 25–30.
- (8) Heneghan, S. P.; Knoot, P. A.; Benson, S. W. The Temperature Coefficient of the Rates in the System  $\text{Cl} + \text{CH}_4 = \text{CH}_3 + \text{HCl}$ , Thermochemistry of the Methyl Radical. *Int. J. Chem. Kinet.* **1981**, *13*, 677–691.

- (9) Seeley, J. V.; Jayne, J. T.; Molina, M. J. Kinetic Studies of Chlorine Atom Reactions Using the Turbulent Flow Tube Technique. *J. Phys. Chem.* **1996**, *100*, 4019–4025.
- (10) Pilgrim, J. S.; McIlroy, A.; Taatjes, C. A. Kinetics of Cl Atom Reactions with Methane, Ethane, and Propane from 292 to 800 K. *J. Chem. Phys. A.* **1997**, *101*, 1873–1880.
- (11) Bryukov, M. G.; Slagle, I. R.; Knyazev, V. D. Kinetics of Reactions of Cl Atoms with Methane and Chlorinated Methanes. *J. Chem. Phys. A.* **2002**, *106*, 10532–10542.
- (12) Allison, T. C.; Truhlar, D. G. In *Modern Methods for Multidimensional Dynamics Computations in Chemistry*; Thompson, D. L., Ed.; World Scientific: Singapore, 1998; pp 618–712.
- (13) Nandi, A.; Bowman, J. M.; Houston, P. A Machine Learning Approach for Rate Constants. II. Clustering, Training, and Predictions for the  $\text{O}(^3\text{P}) + \text{HCl} \rightarrow \text{OH} + \text{Cl}$  Reaction. *J. Phys. Chem. A.* **2020**, *124*, 5746–5755.
- (14) Hoppe, H.; Manthe, U. First-Principles Theory for the Reaction of Chlorine with Methane. *J. Phys. Chem. Lett.* **2022**, *13*, 2563–2566.
- (15) Georgievskii, Y.; Klippenstein, S. J. Entanglement Effect and Angular Momentum Conservation in a Nonseparable Tunneling Treatment. *J. Chem. Theory Comput.* **2021**, *17*, 3863–3885.
- (16) McDowell, R. S. Rotational Partition Functions for Spherical-top Molecules. *Journal of Quantitative Spectroscopy and Radiative Transfer* **1987**, *38*, 337–346.
- (17) McDowell, R. S. Rotational Partition Functions for Symmetric-top Molecules. *J. Chem. Phys.* **1990**, *93*, 2801–2811.
- (18) Herzberg, G. *Infrared and Raman Spectra of Polyatomic Molecules*; Molecular Spectra and Molecular Structure: II. Infrared; D. Van Nostrand: London, 1945; p 508ff.